A prediction model for snowmelt, snow surface temperature and freezing depth using a heat balance method

doi: 10.1175/1520-0450(1990)029<0375:APMFSS>2.0.CO;2

A Prediction Model for Snowmelt, Snow Surface Temperature and Freezing Depth Using a Heat Balance Method

JUNSEI KONDO AND TAKESHI YAMAZAKI

Geophysical Institute, Tohoku University, Sendai, Japan

(Manuscript received 12 June 1989, in final form 10 October 1989)

ABSTRACT

A snowmelt model based on a heat balance method has been developed. This model takes into account both the heat balance at the snow surface and that of the entire snow cover and simultaneously predicts the snow surface temperature and freezing depth. Observed or estimated incident radiation data are required for operation of the model.

Calculated amounts of snowmelt and snow surface temperatures were in agreement with those observed. Dependency of snowmelt on several parameters including maximum liquid water content, thermal conductivity and albedo of the snow was examined. It was found that as liquid water content or thermal conductivity increases, snowmelt decreases. Albedo is very influential in evaluating snowmelt.

Runoff from a basin having an area of 583 km^2 was estimated using the present model, and was verified by the inflow data to a dam.

1. Introduction

The evaluation of snowmelt is not only important in the effective utilization of water resources and the forecasting of flood runoff, but it also influences climate through the change in ground surface properties. The amount of snowmelt can be predicted if the energy exchange through the snow surface can be evaluated. The principal terms of the energy exchange are solar radiation, downward atmospheric radiation, emission from the snow surface and both sensible and latent heat fluxes. Several studies have measured sensible and latent heat fluxes directly (e.g., McKay and Thurtell 1978); however, there are few regular observations of solar and/or downward atmospheric radiation. In practice, the components of the energy exchange are usually estimated from routine meteorological data (Anderson 1968; Föhn 1973; Price and Dunne 1976; Granger and Male 1978). Investigations of the energy exchange over snow surfaces were reviewed by Male and Granger (1981). Recently, Berris and Harr (1987) studied the heat balance of snow surfaces in forested and clear-cut sites during rainfall. Kuhn (1987) investigated the conditions at the onset or the end of melting through theoretical considerations and showed that snow could melt at air temperature as low as −10°C and might stay frozen at +10°C. Air temperature is not the only parameter to determine the amount of snowmelt.

Kondo and Yamazaki (1987) proposed a simple model based on a heat balance method to evaluate snowmelt from routinely obtained meteorological data. In their model, however, it was assumed in principle that the snow surface temperature was equal to 0°C.

During the snowmelt season, the entire snow cover is almost isothermal at 0°C, but the free water near the snow surface may refreeze due to nocturnal cooling. The depth to which the refreezing occurs is termed the "freezing depth" in this paper. de La Casinière (1974) pointed out that refreezing is important in order to make an accurate estimate of the runoff.

The present model simultaneously calculates the snow surface temperature and freezing depth, taking into consideration the nocturnal refreezing of liquid water in the snow cover. Part of the incident solar radiation is transmitted into the interior of the snow cover, which is also considered in this model. The sensible and latent heat fluxes are parameterized by bulk formulas and a linear temperature profile is assumed in the snow cover. Thus the heat balance equations both for the snow surface itself and for the entire snow cover are solved. It is not necessary to perform an iteration of the calculations.

In the present paper it is found that, at a flat site, this model can predict the amount of snowmelt and snow surface temperature. Further, when the model is applied to a drainage area of 583 km^2, the total amount of snowmelt is compared with the runoff measured at the site of a dam with favorable results.

2. Model

a. Basic equations

Schematic profiles of the snow temperature T and water content W are shown in Fig. 1. The depth Z,

Corresponding author address: Prof. Junseio Kondo, Geophysical Institute, Tohoku University, Sendai 980, Japan.

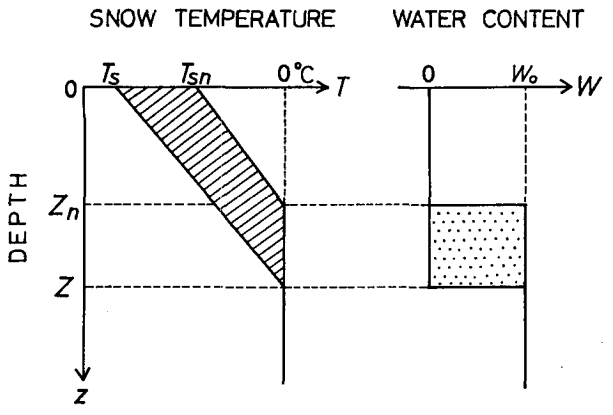

FIG. 1. Schematic snow temperature and water content profiles in the model.

where the straight line of the temperature profile intersects $T = 0°C$ represents the freezing depth. According to a numerical experiment the vertical profiles of snow temperature can be approximated by straight lines (see appendix A). It should be noted that this approximation of snow temperatures does not apply to the midwinter when the snow temperature falls below the freezing point in the lower layer of the snow cover.

Liquid water content W is assumed as

$$\left.\begin{aligned} W &= 0 \quad (z < Z) \\ W &= W_0 \quad (z \geqq Z), \end{aligned}\right\} \tag{1}$$

where W_0 is the maximum water content. Water content is defined as the ratio of the mass of liquid water to the mass of the wet snow. Equation (1) denotes that the layer contains no liquid water where $z < Z$ since the snow temperature is lower than the freezing point, whereas where $z \geqq Z$, it contains as much liquid water as possible.

After an amount of time equivalent to the length of a time step Δt passes, the snow surface temperature T_S has changed to T_{Sn} and Z now equals Z_n, then the equation for the conservation of energy for the entire snow cover can be written as (see Fig. 1)

$$\frac{1}{2} C_S \rho_S [Z(T_0 - T_S) - Z_n(T_0 - T_{Sn})] + W_0 \rho_S l_f (Z - Z_n) + M_0 \Delta t = G \Delta t. \tag{2}$$

Here, $T_0 = 0°C$ and l_f is the heat of fusion for ice. The first term on the left-hand side of (2) describes the energy associated with heating or cooling of the snow (the shaded portion in Fig. 1) while the second term accounts for the energy of fusion or freezing of the liquid water remaining in snow cover (the stippled portion in Fig. 1). In the third term, M_0 is the energy required to create runoff from the snow cover in surplus of the maximum water content. On the right-hand side, G represents the energy received by the entire snow cover through the snow surface and bottom, and is given by

$$G = R - \epsilon \sigma T_S^4 - H - lE + Q_R + Q_B, \tag{3}$$

where R is the incident radiation, written as

$$R = (1 - \alpha) S^{\downarrow} + \epsilon L^{\downarrow}. \tag{4}$$

Snow albedo α, solar radiation $S^{\downarrow}$ and downward atmospheric radiation $L^{\downarrow}$ are either measured or estimated; σ is the Stefan–Boltzmann constant. The value $\epsilon = 0.97$ is used for the snow emissivity (Kondo and Yamazawa 1986a), and H, lE, Q_R and Q_B are the sensible heat flux, the latent heat flux, the heat flux due to rain and the ground heat flux, respectively.

The sensible heat H and latent heat lE are given by the following bulk formulas:

$$H = C_P \rho C_H U (T_S - T_a), \tag{5}$$

$$lE = l\rho C_E U (q_s(T_S) - q) \fallingdotseq l\rho C_E U[(1 - h) q_s(T_a) + \Delta \cdot (T_S - T_a)], \tag{6}$$

where C_P and ρ are the specific heat of air at constant pressure and air density, respectively. Here U, T_a, q and h represent the wind speed, air temperature, specific humidity and relative humidity, respectively, measured at a given reference height. The value $q_s(T)$ is the saturated specific humidity at temperature T, while $\Delta = dq_s/dT$ at T_a. The bulk coefficients for sensible and latent heat are given by C_H and C_E, respectively. Kondo and Yamazawa (1986b) obtained values of $C_H = 0.002$ and $C_E = 0.0021$ over a flat snow surface at a reference height of 1 m and suggested that they are practically independent of wind speed. These values are also chosen for use in the present study.

It is difficult to estimate the heat due to rain Q_R, however. The Q_R is small in general, for example, 10 mm rain at 10°C can melt only 1.25 mm snow in water equivalent. The ground heat flux Q_B is also small—less than 1 mm d^{-1} in snowmelt except for early winter (e.g., Kojima and Motoyama 1985). Therefore, Q_R and Q_B are ignored in this paper.

The heat balance equation of a snow surface with an infinitesimal thickness is schematically represented in Fig. 2 and can be written as

$$\epsilon(L^{\downarrow} - \sigma T_{Sn}^4) - H - lE + \lambda_S \frac{T_0 - T_{Sn}}{Z_n} = 0, \tag{7}$$

where λ_S is the thermal conductivity of snow. Note that since snow transmits solar radiation, (7) includes no terms associated with solar radiation. Expanding T_{Sn}^4 around the air temperature T_a and substituting (5) and (6) with $T_S = T_{Sn}$, (7) becomes

$$\epsilon(L^{\downarrow} - \sigma T_a^4) - (4\epsilon\sigma T_a^3 + C_P \rho C_H U + l\rho C_E U \Delta)(T_{Sn} - T_a) - l\rho C_E U (1 - h) q_s(T_a) + \lambda_s \frac{T_0 - T_{Sn}}{Z_n} = 0. \tag{8}$$

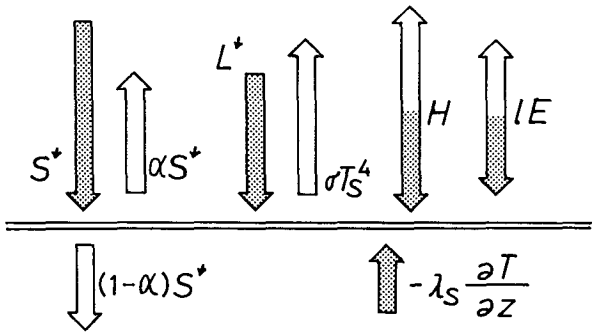

FIG. 2. Schematic of the heat balance for a snow surface.

In (7) and (8) T_a, h, U and $L^{\downarrow}$ are known values when $Z = Z_n$ and $T_S = T_{Sn}$. For the specific case when the net radiation R_n is given in place of $L^{\downarrow}$, the reader is referred to appendix B.

By solving (2) and (8), it is possible to obtain the snow surface temperature, freezing depth and snowmelt simultaneously.

b. Practical method of calculation

The practical method of the solution is shown in exact form in the following (see also Fig. 3 for a flow chart). First, it is considered that $M_0 = 0$ in (2). Elimination of T_{Sn} by combining (2) and (8) gives the following quadratic equation:

$$A_2 Z_n^2 + A_1 Z_n + A_0 = 0, \tag{9}$$

where

$$A_2 \equiv C_1[\epsilon(L^{\downarrow} - \sigma T_a^4) + C_2(T_a - T_0) - l\rho C_E U(1 - h)q_s(T_a)] - C_2 C_3,$$

$$A_1 \equiv [C_3 Z + C_1 Z(T_0 - T_S) - G\Delta t]C_2 - C_3\lambda_S,$$

$$A_0 \equiv \lambda_S[C_3 Z + C_1 Z(T_0 - T_S) - G\Delta t],$$

$$C_1 \equiv C_S\rho_S/2,$$

$$C_2 \equiv 4\epsilon\sigma T_a^3 + C_P\rho C_H U + l\rho C_E U\Delta$$

and

$$C_3 \equiv W_0\rho_S l_f.$$

The meaningful solution of (9) is given by

$$Z_n = \frac{-A_1 - (A_1^2 - 4A_2A_0)^{1/2}}{2A_2}. \tag{10}$$

Values of Z_n are allowed in the range of $Z_{\min} \leqq Z_n \leqq d$, where d is the snow depth. The constant $Z_{\min}$ is determined to be a small value, with $Z_{\min} = 1$ cm used in the present calculation ($Z_{\min} = 0.1$ cm yields almost the same results). Here $Z_{\min} = 0$ was not used to avoid the divergence of the last term on the left side of (8). The following conditions are assumed for finding Z_n. If the solution of Z_n lies in the region $Z_n < Z_{\min}$ (including $Z_n < 0$), Z_n is set equal to $Z_{\min}$. When $Z_n > d$, then the value is determined by $Z_n = d$. The value of T_{Sn} is obtained by substituting this value of Z_n in (8).

When $T_{Sn} > 0$°C, it is replaced by 0°C and Z_n is further recalculated by the following equation:

$$Z_n = Z + \frac{C_1 Z(T_0 - T_S) - G}{C_3}. \tag{11}$$

Thus, Z_n and T_{Sn} are determined.

In the case of $Z_{\min} < Z_n \leqq d$, because Z_n and T_{Sn} satisfy (2) with $M_0 = 0$, no snowmelt occurs. For the case of $Z_n = Z_{\min}$, M_0 is obtained by the substitution

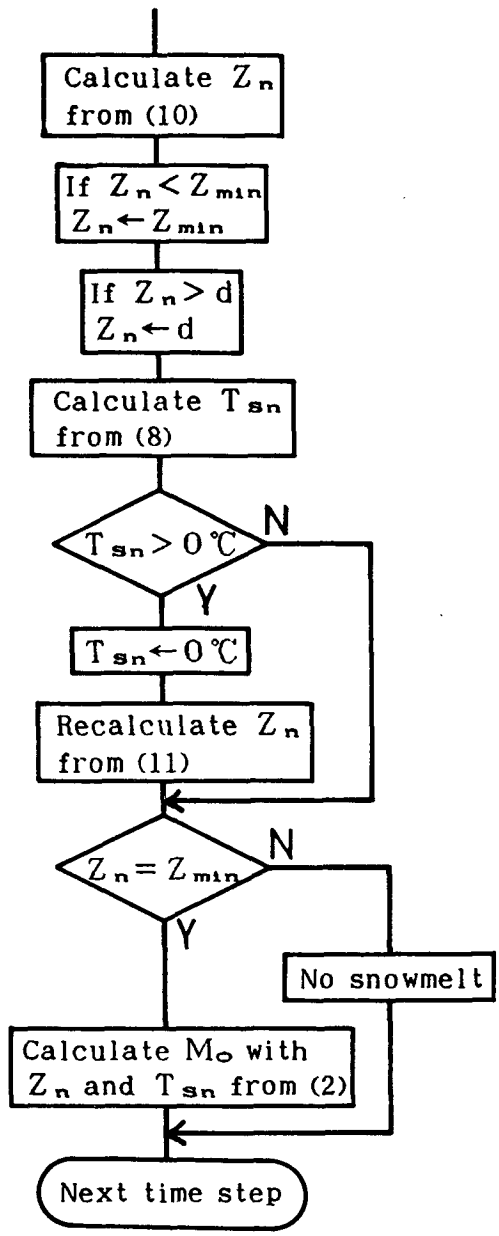

FIG. 3. Algorithm of the snowmelt model.

of Z_n and T_{Sn} into (2). This calculation determines the amount of runoff for this time step.

With these results, the calculation falls back to (10) and proceeds from there. The time step is constant, set at Δt = 1 hour.

3. Simulation of the snowmelt process

Incident solar radiation, reflected solar radiation, atmospheric radiation, wind speed, air temperature and humidity were observed during the spring of 1986 over the flat farmland of Tohoku University in Kawatabi, Miyagi Prefecture, Japan. Liquid water content of the snow below the freezing layer was measured as 6%–16% by a calorimeter designed by Yosida (1960). With the use of these values, the maximum water content was set at $W_0 = 0.1$, and the thermal conductivity at $\lambda_S = 0.42$ W m^{-1} K^{-1}, since the snow is considered to be high density granular snow (Kondo 1988). The snowmelt process is simulated from these data, and the results are compared with those observed. The water equivalents and densities of the snow cover were measured by a cylindrical snow sampler 0.5–1.5 m long. The range of observed snow densities was from 0.29 to 0.41 g cm^{-3}.

Figure 4 displays the time variation of both the calculated and observed water equivalents, with the observed values indicated by circles. In this calculation, the observed water equivalent of 6 March is used for the initial condition. The actual snowmelt is reproduced rather well, as can be seen in this example.

Calculated snow surface temperatures are also compared with observed values that were measured by an infrared radiation thermometer. An example for results of 12–13 March is shown in Fig. 5, along with the heat balance components. As can be seen, there is a fairly good correspondence between the observed temperature (dashed line) and the calculated value (solid line).

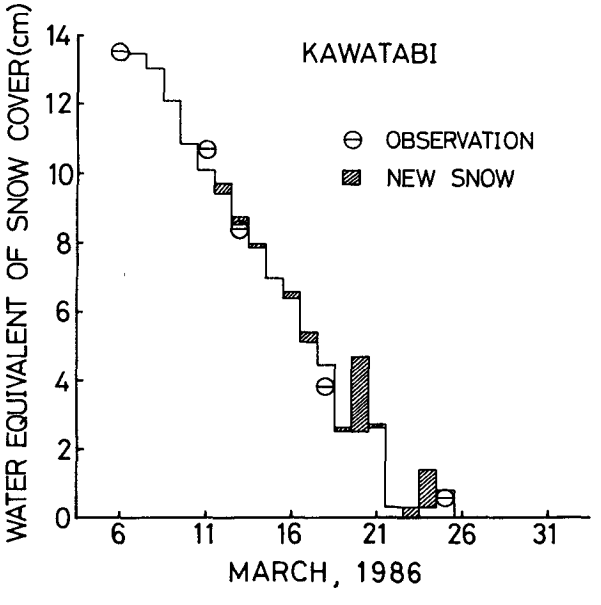

FIG. 4. An example of simulated water equivalent of snow cover. Circles denote observed water equivalent and the hatched portion denotes an increase in water equivalent to new snowfall.

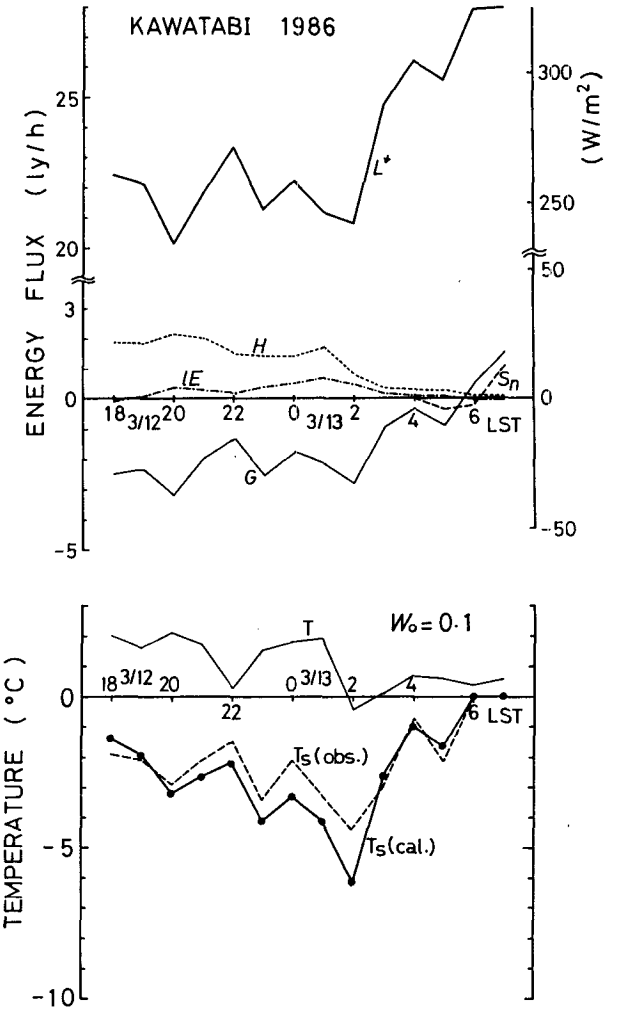

FIG. 5. Time variation in snow surface temperature (lower panel) and heat balance components (upper panel).

The snow surface temperature T_S varies in phase with the energy received through the snow surface G and the atmospheric radiation $L^{\downarrow}$. Since the sky was clear until about 0300 LST during this period, the snow surface temperature decreased with time through radiative cooling. After 0300 LST it became cloudy at the site, and T_S increased suddenly. The present results show that the snow surface temperature is predictable to within 1°C.

4. Dependence of snowmelt on water content, thermal conductivity and the albedo of snow

The estimated snowmelt depends on the value of maximum water content W_0, thermal conductivity λ_S

and the snow albedo α, the relationship among which is now examined. For this purpose an examination was carried out under the same meteorological conditions during the period 6–18 March 1986 at Kawatabi. The water equivalent of the observed snowmelt was 10.8 cm during this period.

a. Maximum water content

The dependence of snowmelt on the maximum water content is given in Fig. 6, which shows that as the water content increases the snowmelt decreases; this can be explained as follows. Since the nocturnal freezing depth decreases as the maximum water content increases, the snow surface temperature does not fall. Therefore, as the energy loss through infrared emission increases, the snowmelt decreases with an increase in the maximum water content.

It is difficult to obtain an exact value for the maximum water content. Fortunately, the dependence of snowmelt on water content is weak for $W_0 \geqq 0.05$; however, the dependence is rather strong for $W_0 \fallingdotseq 0$, making it unfavorable to assume that the model contains no water.

b. Thermal conductivity

The dependence of snowmelt on the thermal conductivity of the snow is shown in Fig. 7; as the thermal conductivity increases the snowmelt decreases. This is because the nocturnal decrease of the snow surface temperature is small for a large thermal conductivity. The value of λ_s can be expressed in terms of the snow density ρ_S (e.g., Kondo 1988), which may differ for various snow types. Therefore, the thermal conductivity should be determined in advance from observed or estimated snow density.

c. Albedo

Figure 8 plots the calculated snowmelt versus the albedo of the snow cover, showing that the snowmelt is very sensitive to the albedo. In the following, a parameterization of the snow albedo is used.

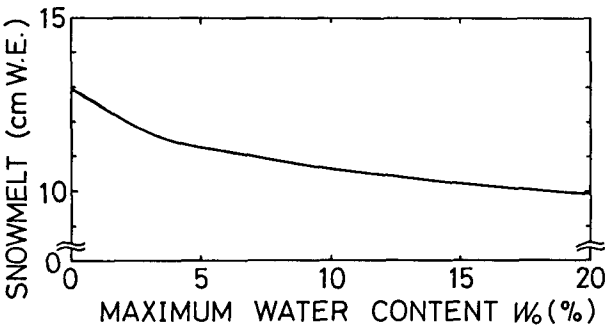

FIG. 6. Dependence of snowmelt on maximum water content (at Kawatabi, 6–18 March), for the same conditions as in Fig. 4.

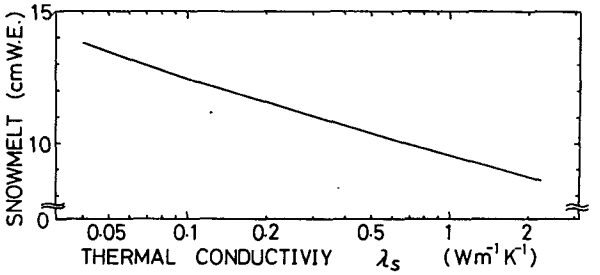

FIG. 7. Dependence of snowmelt on snow thermal conductivity, for the same conditions as in Fig. 4.

The observed mean albedo during the period of 6–18 March was 0.686. It is interesting that the snowmelt that corresponds to this mean albedo almost agrees with actual snowmelt 10.8 cm.

5. Estimate of the runoff from a drainage basin

The present model is applied to a drainage basin of a heavy snowfall region, one that reaches a mean snow depth of 2 m during the winter. Yuda dam is located at the outflow of this drainage basin at the head of the Waga River (Fig. 9). The amount of predicted inflow to Yuda dam was calculated for 1965, 1974 and 1985. Details of the meteorological data are given in Kondo and Yamazaki (1987).

The drainage basin is divided into three regions, shown separated by the dotted lines in Fig. 9. These regions are represented by "Yuda," "Sawauchi" and "Wakahata," respectively, where meteorological data are obtained. Each region is subdivided into layers that differ by an interval of 200 m in elevation. The amount

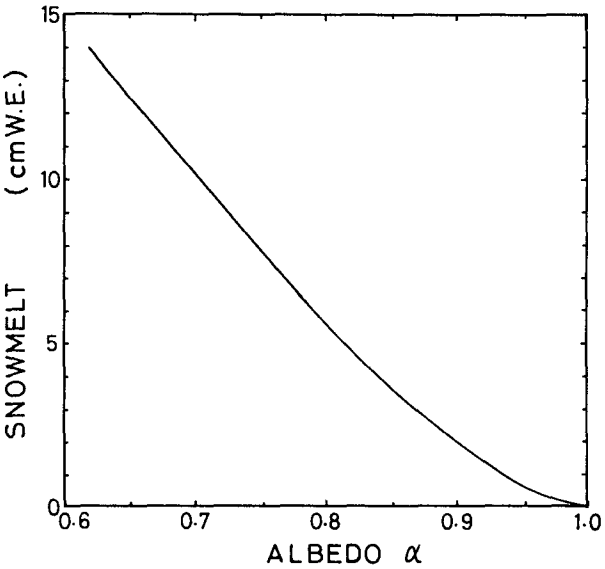

FIG. 8. The relation between albedo and snowmelt, for the same conditions as in Fig. 4.

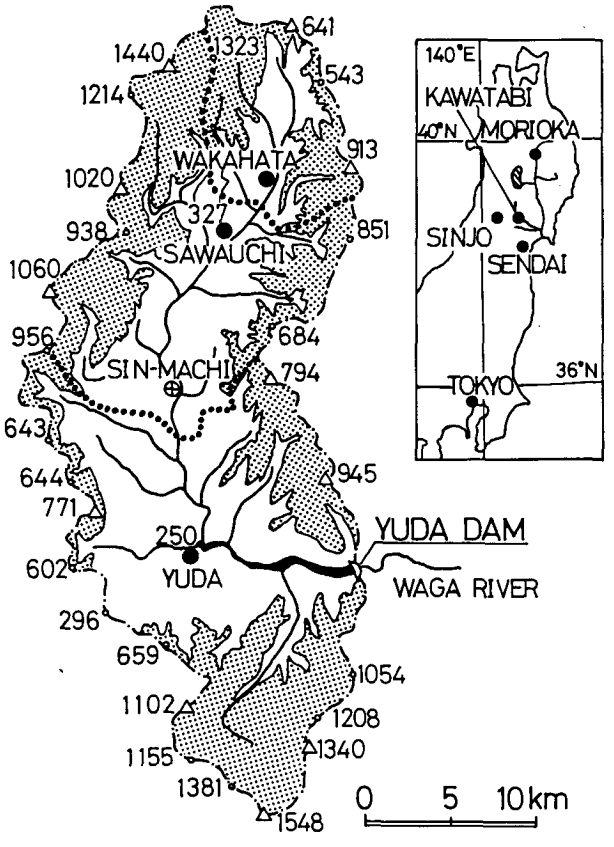

FIG. 9. Location of the test basin, Tohoku district, Japan. Stippled area denotes greater than 500 m above sea level, the dash-dotted line defines the watershed, the dotted lines separate the boundaries of regions.

of snowmelt for each subdivision is calculated with the assumption of a temperature lapse rate 0.0065°C m^{-1}.

With reference to Kondo et al. (1988), the albedo is assumed to decrease exponentially with time (days) that has passed since the last snowfall as

$$\alpha(n) = \alpha_{\min} + (\alpha(0) - \alpha_{\min})e^{-n/K}, \qquad (12)$$

where $\alpha(n)$ is the albedo for the nth day from the last snowfall, $\alpha_{\min}$ the converged value of the albedo and K a parameter representing the rate of decrease. The value of $\alpha_{\min} = 0.4$ is chosen, which is a measured value for early April 1985 at Sawauchi (already in melting season) and $K = 4$ days is used. If the daily mean temperature is less than 1°C and the amount of precipitation is more than 3 mm d^{-1}, it is assumed that the surface is covered by fresh snow, and n is reset to zero. The value of $\alpha(0)$ is assumed to be 0.85 for this study. The albedo changes as it jumps to a maximum value when the surface is covered by fresh snow, it then decreases exponentially until the next fresh snowfall. Maximum water content and thermal conductivity are the same as those found in section 3; i.e., $W_0 = 0.1$ and $\lambda_S = 0.42$ W m^{-1} K^{-1}.

As previously mentioned, when the daily mean temperature is less than 1°C, the precipitation is assumed to take the form of snow and its water equivalent is added to the water equivalent of the snow cover. On the other hand, for rain, it is assumed to flow out as runoff. For both forms of precipitation the observed values at each representative site along with the correction coefficient b for the distribution of the precipitation is used (see appendix C). When the snow cover was no longer present, a value of 2 mm day^{-1} for the evaporation from the ground was assumed, with this value being subtracted from the calculated runoff.

According to Yamada (1983) and Koike et al. (1986), initial snow water equivalent is given by a linear function of elevation as

$$x_i(y) = \gamma(y - y_{i0}) + x_{i0}, \qquad (13)$$

where y and y_{i0} are the elevation of the considered and representative points, respectively and x_{i0} is the initial snow water equivalent at each representative point. The proportional coefficient γ is estimated every year using the inflow data to the dam and precipitation during snowmelt to the summer seasons. A linear relationship is found between γ and initial snow depth at each representative point [appendix C, (A16) and Fig. A4]. This relationship is useful when γ is unknown.

The results are shown in Fig. 10. Estimated runoff roughly agrees with that observed. The inflow to the dam increases gradually at first, and reaches a maximum at the end of April or in early May. Then the inflow decreases as the snow covered area decreases, to the point where the snow is completely gone at the bottom of the drainage basin.

Due to the overestimate of runoff during 6–10 April 1965 and 1–5 May 1974, it subsequently may have occurred that the runoff was underestimated during 21–26 May in both years.

Figure 11 shows the area-averaged contribution for each heat balance component to the snowmelt. They are obtained by accumulating the values during the period when $M_0 \geqq 0$ (snowmelt season). Sensible and latent heat fluxes are important during May as the air warms, but radiation still accounts for 65%–70% of the total energy on the average for May.

Two problems may exist in the calculation of the inflow to the dam. The first is how representative the components are, such as solar radiation, wind velocity, precipitation and the amount of snow cover at the observation sites. Also, the heat balance may vary with the surface features, e.g., forest, bare ground and local topography. Hence, the location of the snowmelt may strongly affect the outcome. A good question is why the calculated snowmelt almost agrees with the actual inflow to the dam. In future research this agreement should be clarified by taking account of the variety of ground surfaces and the complexity of the terrain.

The second problem is that no mechanisms for meltwater penetration into the ground and time lag in run-

off are included in the scheme. This was one reason the comparisons are carried out over an interval of five days in this paper. It is necessary to take into consideration these mechanisms to predict runoff for shorter intervals such as one day, a half day or even one hour.

6. Summary

The model of snowmelt was developed on the basis of a heat balance of the snow surface and the energy conservation of the entire snow cover with an assumption of a linear temperature profile in the snow. The model predicts the amount of snowmelt, the heat balance components, the snow surface temperature and freezing depth. The following components are necessary as the input data to the model: the solar radiation, downward longwave radiation, wind velocity, air temperature and humidity. Also, for the parameters of snow cover: the albedo, density, water content and thermal conductivity need to be known prior to the calculation.

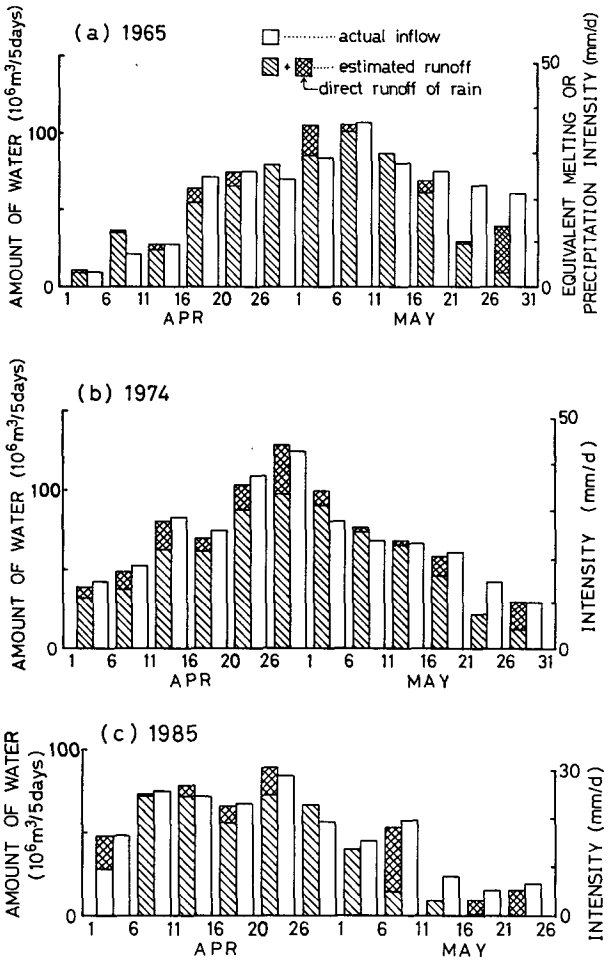

FIG. 10. Estimated and actual inflow to the dam. Increasing rates of water equivalent with elevation are (a) for 1965, $\gamma = 3.4 \times 10^{-4}$ m m^{-1}, (b) for 1974, $\gamma = 6.9 \times 10^{-4}$ m m^{-1}, (c) for 1985, $\gamma = 6.2 \times 10^{-4}$ m m^{-1}.

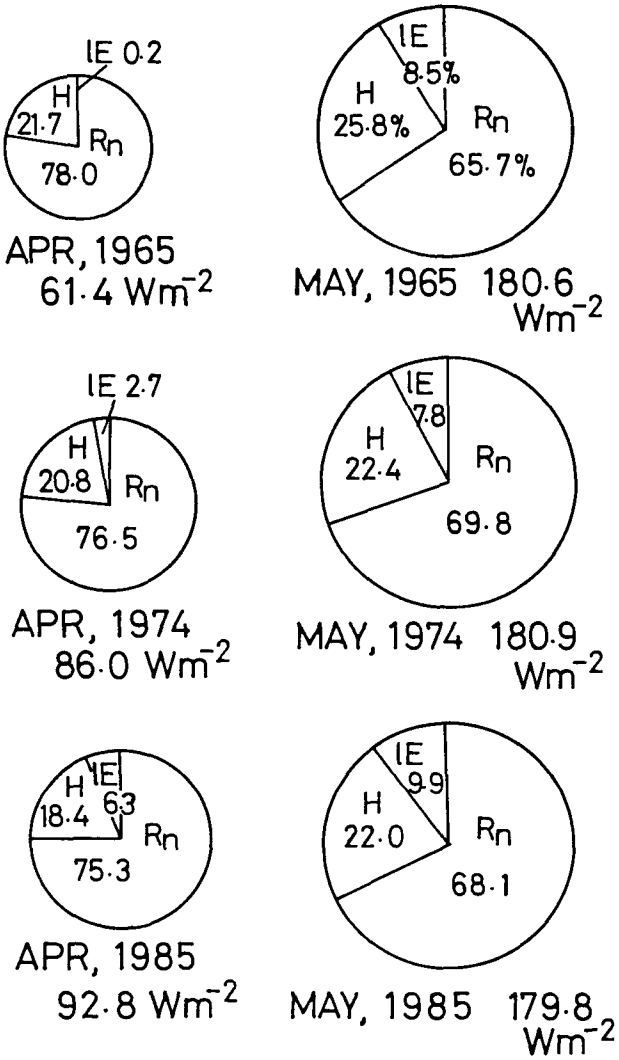

FIG. 11. Area-averaged contribution of each heat balance component to snowmelt. Left: for April, Right: for May.

The simulated process of snowmelt agrees well with observations made over a flat farmland. Moreover, the calculated snow surface temperature corresponds with the actual value.

As the maximum water content or thermal conductivity increases, the calculated snowmelt decreases. The reason for this is that the snow surface temperature is kept higher during the nighttime for larger maximum water content and thermal conductivity. Snowmelt largely depends on albedo.

Finally, the model was applied to a large area to estimate the inflow to a dam. In this calculation, it was assumed that the initial snow water equivalent increased linearly with altitude. The predicted values of inflow are consistent with those observed.

Acknowledgments. The authors wish to thank Professor T. Abe and the staff of the farmland of Tohoku University for their cooperation during the observations. They also would like to thank their colleagues at Tohoku University for assistance in the observations and for valuable comments.

APPENDIX A

Temperature Profiles in Snow Layer (Model Experiment)

The z axis is taken in the downward direction. The snow temperature T is governed by the following equation:

$$C_S\rho_S\frac{\partial T}{\partial t} = \lambda_S\frac{\partial^2 T}{\partial z^2} + \mu I\exp(-\mu z) - l_f F, \quad \text{(A1)}$$

where C_S, ρ_S and λ_S are specific heat, density and thermal conductivity of the snow cover, respectively. Here μ is the extinction coefficient of solar radiation within the snow cover, $I = (1-\alpha)S^{\downarrow}$ is the incident solar radiation at the snow surface and F is the amount of snowmelt per unit time and unit volume. At the snow surface, it holds that

$$C_S\rho_S\frac{\partial T_S}{\partial t}dz = \lambda_S\left(\frac{\partial T}{\partial z}\right)_{z=0} + (\mu I\exp(-\mu z) - l_f F)dz + \epsilon L^{\downarrow} - \epsilon\sigma T_S^4 - H - lE. \quad \text{(A2)}$$

The differential forms of (A1) and (A2) are:

$$T_{n+1,i} = \frac{\lambda_S\Delta t}{C_S\rho_S(\Delta z)^2}(T_{n,i-1} - 2T_{n,i} + T_{n,i+1}) + \frac{\Delta t}{C_S\rho_S}(\mu I\exp(-\mu z) - l_f F) + T_{n,i}, \quad \text{(A3)}$$

$$T_{n+1,1} = \frac{\lambda_S\Delta t}{C_S\rho_S(\Delta z)^2}(T_{n,2} - T_{n,1}) + \frac{\Delta t}{C_S\rho_S}(\mu I\exp(-\mu z) - l_f F) + \frac{\Delta t}{C_s\rho_S\Delta z} \times (\epsilon L^{\downarrow} - \epsilon\sigma T_{n,1}^4 - H - lE) + T_{n,1}, \quad \text{(A4)}$$

where the first suffix n denotes the time step and the second suffix i represents the grid point (Fig. A1). Here $i = 1$ indicates the uppermost layer in contact with the air. Maximum water content, W_0, is the same for any layer. Sensible and latent heat fluxes are given by

$$H = C_P\rho C_H U(T_{n,1} - T_{1\,\mathrm{m}}) \quad \text{(A5)}$$

and

$$lE = l\rho C_E U(q_s(T_{n,1}) - q_{1\,\mathrm{m}}). \quad \text{(A6)}$$

Here $T_{1\,\mathrm{m}}$ and $q_{1\,\mathrm{m}}$ are the air temperature and specific humidity at 1 m above the snow surface, respectively, and U and $T_{1\,\mathrm{m}}$ are determined from daily averaged data by applying a typical pattern of diurnal variation. The diurnal variation of $q_{1\,\mathrm{m}}$ is not considered. The diurnal variation of $S^{\downarrow}$ is given by an empirical formula following Kondo and Miura (1985), and $L^{\downarrow}$ is assumed to be constant. Kondo and Yamazaki (1987) have described how to determine U, $T_{1\,\mathrm{m}}$, $S^{\downarrow}$ and $L^{\downarrow}$ in more detail.

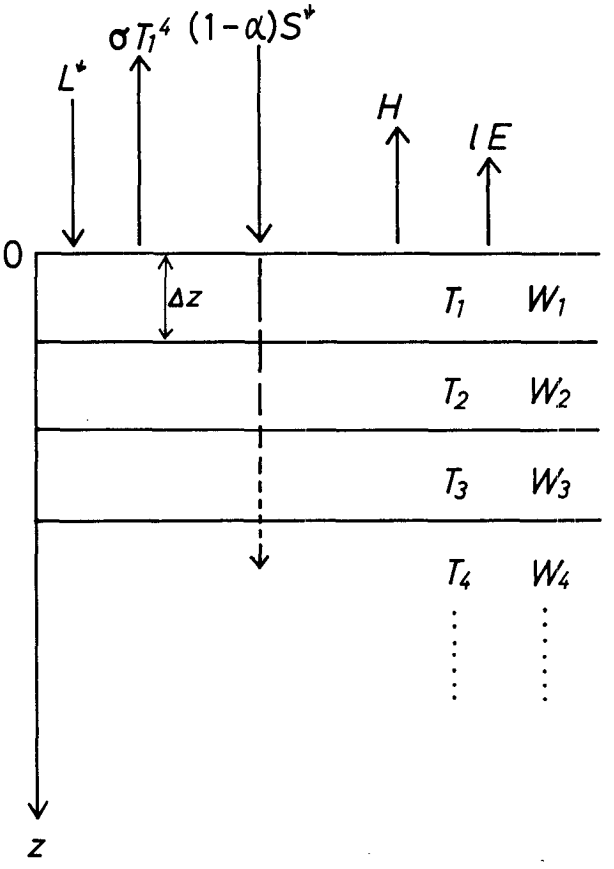

FIG. A1. Schematic of snow cover used to calculate snow temperature profiles.

Snowmelt occurs only under the condition that $T = 0°C$. Therefore, the calculating procedure changes according to $T_{n,1}$ being equal to 0°C or not. The flow chart of the procedure is shown in Fig. A2.

Initially (at noon), for calculation purposes the snow temperature is set to 0°C with the water content at the maximum value for each layer. In the model calculation for the snowmelt season the constants are assumed as follows:

$$\Delta z = 2\ \mathrm{mm},$$
$$C_s\rho_s = 8.4\times10^5\ \mathrm{J\ m^{-3}\ K^{-1}},$$
$$\lambda_s = 0.42\ \mathrm{W\ m^{-1}\ K^{-1}},$$
$$\mu = 40\ \mathrm{m^{-1}},$$
$$\alpha = 0.4,$$
$$W_0 = 0.05,$$

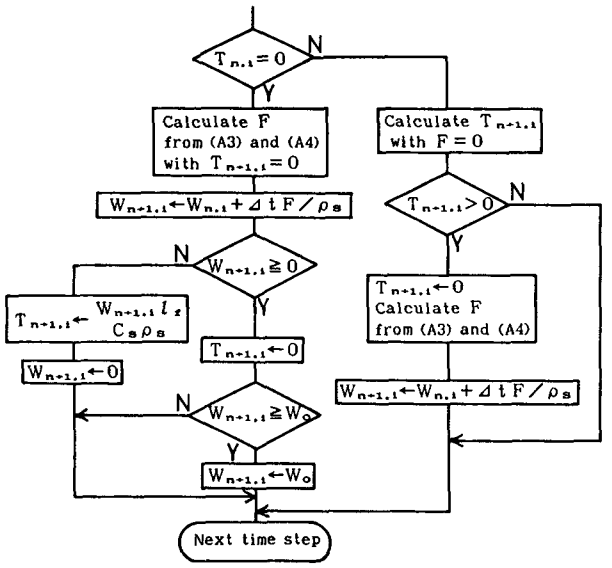

FIG. A2. Algorithm used for calculating the snow temperature and water content. $W_{n,i}$: water content of the ith layer, W_0: maximum water content.

mean air temperature = 0°C
(daily amplitude = 5°C),
minimum humidity = 60%,
$U = 2$ m s^{-1},
$S^{\downarrow}_{max} = 728$ W m^2,
$L^{\downarrow} = 231$ W m^{-2}.

The value of μ for wet snow is taken from Fukami et al. (1985).

The results for a given day in spring are shown in Fig. A3. Even if U, $S^{\downarrow}_{max}$ and/or $L^{\downarrow}$ are changed, similar shapes of the temperature profile are obtained (figures not shown). As the air temperature increases during the morning, the snow temperature first reaches 0°C at a certain depth below the surface (internal melting). This is due to the transmission of solar radiation to within the snow cover. Since the snow surface temperature is less than 0°C when internal melting occurs, the energy loss by infrared radiation is smaller than when $T_S = 0$°C. Therefore, the net radiation received by the snow cover becomes greater.

The temperature profiles within the snow can be linearly approximated except for during a few hours in the morning when internal melting occurs. In this study, it was assumed that the linear temperature profiles within the snow are as shown in Fig. 1.

APPENDIX B

When the Net Radiation Data is Given

Net radiation is rather sensitive to the ground surface temperature and has a regional variability. Incident radiation, however, does not vary regionally to any great extent to that its value can be estimated for an extensive area from given meteorological data at an observation site. Therefore, it is prudent to use the incident radiation R as an external parameter rather than the net radiation R_n. In practice, however, net radiation is often measured. If R_n is measured instead of $L^{\downarrow}$, the following equation can be used instead of (8):

$$-L_n - (C_P\rho C_H U + l\rho C_E U\Delta)(T_{Sn} - T_a) - l\rho C_H U(1-h)q_s(T_a) + \lambda_s \frac{T_0 - T_{Sn}}{Z_n} = 0. \quad \text{(A7)}$$

Here, L_n is the net infrared radiative flux:

$$L_n = \sigma T_S^4 - L^{\downarrow} = (1-\alpha)S^{\downarrow} - R_n. \quad \text{(A8)}$$

It should be noted that the form of the equations are the same except that $L^{\downarrow} - \sigma T_a^4$ and C_2 are replaced by $-L_n$ and C_2' ($\equiv C_P\rho C_H U + l\rho C_E U\Delta$).

APPENDIX C

Coefficient for the Elevation Distribution of the Initial Snow Water Equivalent

The distribution of initial snow water equivalent with elevation is necessary to calculate the entire snowmelt over the basin. The total inflow to the dam during the snowmelt season (until the snow is completely gone) D is expressed by

$$D = X_0 + P_0 - ES, \quad \text{(A9)}$$

where X_0 is the initial total snow water equivalent over the basin, P_0 the total precipitation over the basin, E the evaporation which is assumed to be 1 mm day^{-1} and S is the basin area.

It is assumed that P_0 can be expressed as

$$P_0 = b \sum P_i S_i, \quad \text{(A10)}$$

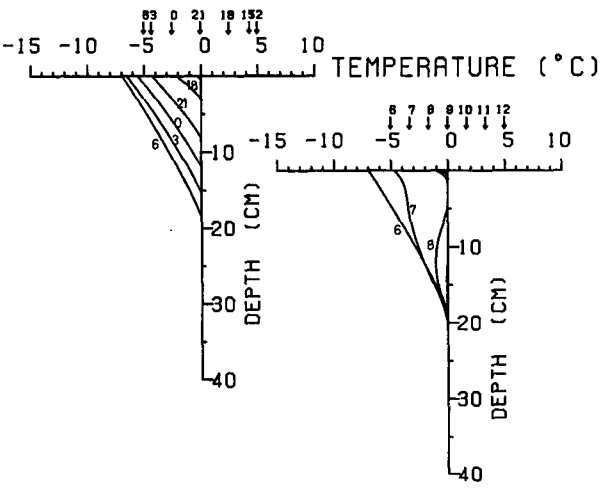

FIG. A3. Diurnal variation of temperature profiles in the snow cover, for a given day with wind speeds of about 2 m s^{-1}. Left panel: cooling period (1200 LST to 600 LST the next morning, 3 hour intervals), right panel: heating period (600 LST to 1200 LST, every hour). The arrows show air temperature at each time.

where the suffix i denotes a region, for example, Yuda or Sawauchi, and P_i is the total precipitation at each observation site during the snowmelt season, S_i is area of each region and b is the correction coefficient.

Next, let the inflow to the dam during the summer season (from June to September) D_S be expressed as

$$D_S = P_{0S} - E_S S, \tag{A11}$$

where suffix S denotes the value for the summer season, and $E_S = 2$ mm d^{-1} is assumed. For the total precipitation P_{0S}, a similar assumption

$$P_{0S} \equiv b \sum_i P_{iS} S_i \tag{A12}$$

is adopted.

With the calculation of b from (A11) and (A12) through the use of observed values of D_S and P_{iS}, X_0 is determined by substituting observed D and P_i into (A10) and (A9).

As the snow water equivalent in northern Japan increases in proportion to height (Yamada 1983; Koike et al. 1986), the following initial water equivalent distribution is assumed:

$$X_0 \equiv \sum x_{ij} S_{ij}, \tag{A13}$$

$$x_{ij} = 200 j\gamma + x_{i0}, \tag{A14}$$

where j is the height increment with a 200 m interval from each representative point ($j = 0, 1, 2, 3$; $j = 0$ denotes the level of the representative observation site). γ is the increasing rate of water equivalent with elevation, x_{ij} is the initial water equivalent for the ith region and jth level, S_{ij} is the area of ith region and jth level and x_{i0} is initial water equivalent at the representative observation site. From (A13) and (A14),

$$\gamma = \frac{X_0 - \sum x_{i0} S_{ij}}{200 \sum j \cdot S_{ij}} \tag{A15}$$

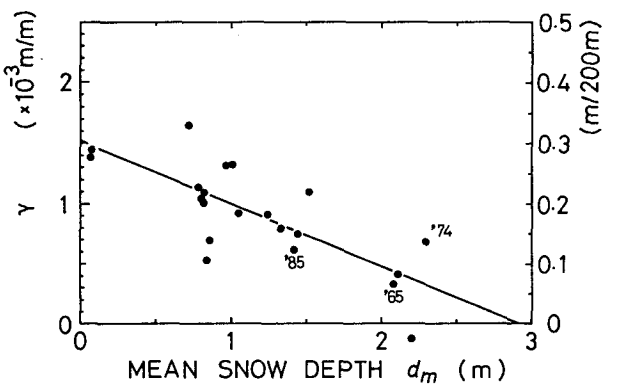

FIG. A4. The relation between snow depth and increasing rate of water equivalent with elevation, γ. The abscissa denotes the average snow depth at Yuda and Sawauchi on 1 April for each year.

can be obtained. By substituting the value of X_0 found from (A9) into (A15), the initial water equivalent distribution can be determined by (A14).

Figure A4 shows the relationship between γ and snow depth for 21 individual years. The value of γ tends to decrease with an increase in snow depth and the following regression equation can be fitted:

$$\gamma = -5.18 \times 10^{-4} d_m + 1.51 \times 10^{-3}. \tag{A16}$$

Here, the unit of γ is m m^{-1} and d_m is the average snow depth (m) at Yuda and Sawauchi on 1 April. The mean value of b was found to be 1.14 (with a standard deviation of 0.10) and is used in section 5.

REFERENCES

Anderson, E. A., 1968: Development and testing of snow pack energy balance equations. *Water Resour. Res.*, **4**, 19–37.

Berris, S. N., and R. D. Harr, 1987: Comparative snow accumulation and melt during rainfall in forested and clear-cut plots in the western Cascades of Oregon. *Water Resour. Res.*, **23**, 135–142.

de La Casinière, A. C., 1974: Heat exchange over a melting snow surface. *J. Glaciol.*, **13**, 55–72.

Föhn, P. M. B., 1973: Short-term snow melt and ablation derived from heat- and mass-balance measurements. *J. Glaciol.*, **12**, 275–289.

Fukami, H., K. Kojima and H. Aburakawa, 1985: The extinction and absorption of solar radiation within a snow cover. *Ann. Glaciol.*, **6**, 118–122.

Granger, R. J., and D. H. Male, 1978: Melting of a prairie snowpack. *J. Appl. Meteor.*, **17**, 1833–1842.

Koike, T., Y. Takahasi and S. Yosino, 1986: Estimation of basin-wide snow water equivalent using snow-covered area. Modelling snowmelt-induced processes *Proc. Budapest Symp., July 1986*, IAHS Publ. no. 155, 193–201.

Kojima, K., and H. Motoyama, 1985: Melting and heat exchange at the bottom of a snow cover. *Ann. Glaciol.*, **6**, 276–277.

Kondo, J., 1988: Parameterizations of thermal conduction, water-vapor transport and flow-down speed of melt water in snow cover. *J. Jpn. Soc. Snow and Ice*, **50**, 17–24. (in Japanese)

——, and A. Miura, 1985: Surface heat budget of the Western Pacific for May 1979. *J. Meteor. Soc. Japan*, **63**, 633–646.

——, Y. Numata and T. Yamazaki, 1988: Parameterization of snow albedo. *J. Jpn. Soc. Snow and Ice*, **50**, 216–224. (in Japanese)

——, and H. Yamazawa, 1986a: Measurement of snow surface emissivity. *Bound.-Layer Meteor.*, **34**, 415–416.

——, and ——, 1986b: Bulk transfer coefficient over a snow surface. *Bound.-Layer Meteor.*, **34**, 123–135.

——, and T. Yamazaki, 1987: Estimates of snowmelt by a heat balance method. *J. Jpn. Soc. Snow and Ice*, **49**, 181–191. (in Japanese)

Kuhn, M., 1987: Micro-meteorological conditions for snow melt. *J. Glaciol.*, **33**, 24–26.

Male, D. H., and R. J. Granger, 1981: Snow surface energy exchange. *Water Resour. Res.*, **17**, 609–627.

McKay, D. C., and G. W. Thurtell, 1978: Measurements of the energy fluxes involved in the energy budget of a snow cover. *J. Appl. Meteor.*, **17**, 339–349.

Price, A. G., and T. Dunne, 1976: Energy balance computations of snowmelt in a subarctic area. *Water Resour. Res.*, **12**, 686–694.

Yamada, T., 1983: Studies on accumulation-ablation processes and distribution of snow in mountain regions, Hokkaido. *Contr. Inst. Low Temp. Sci., A*, **31**, 1–33.

Yosida, Z., 1960: A calorimeter for measuring the free water content of wet snow. *J. Glaciol.*, **3**, 574–576.